Title
Improving Representation of Deforestation Effects on Evapotranspiration in the E3SM Land Model

Journal
Journal of Advances in Modeling Earth Systems, 11(8)

ISSN
1942-2466

Authors
Cai, X
Riley, WJ
Zhu, Q
et al.

Publication Date
2019-08-01

DOI
10.1029/2018MS001551

Peer reviewed

JAMES | Journal of Advances in Modeling Earth Systems

RESEARCH ARTICLE
10.1029/2018MS001551

Special Section:
The Energy Exascale Earth System Model (E3SM)

Improving Representation of Deforestation Effects on Evapotranspiration in the E3SM Land Model

Xitian Cai[1], William J. Riley[1], Qing Zhu[1], Jinyun Tang[1], Zhenzhong Zeng[2,3], Gautam Bisht[1], and James T. Randerson[4]

[1]Climate and Ecosystem Sciences Division, Lawrence Berkeley National Laboratory, Berkeley, CA, USA, [2]School of Environment Science and Engineering, Southern University of Science and Technology, Shenzhen, China, [3]Department of Civil and Environmental Engineering, Princeton University, Princeton, NJ, USA, [4]Department of Earth System Science, University of California, Irvine, CA, USA

Key Points:
- ELMv1 predicted the incorrect sign and magnitude of deforestation effects on evapotranspiration
- Representation of deforestation was improved through model calibration, primarily by changing stomatal resistance and soil water parameters
- The improved model predicted large changes in surface energy budgets associated with deforestation, particularly in tropical rainforests

Supporting Information:
- Supporting Information S1

Correspondence to:
X. Cai,
xtcai@lbl.gov

Citation:
Cai, X., Riley, W. J., Zhu, Q., Tang, J., Zeng, Z., Bisht, G., & Randerson, J. T. (2019). Improving representation of deforestation effects on evapotranspiration in the E3SM land model. *Journal of Advances in Modeling Earth Systems*, *11*, 2412–2427. https://doi.org/10.1029/2018MS001551

Received 5 NOV 2018
Accepted 27 JUN 2019
Accepted article online 2 JUL 2019
Published online 5 AUG 2019

Abstract Evapotranspiration (ET) plays an important role in land-atmosphere coupling of energy, water, and carbon cycles. Following deforestation, ET is typically observed to decrease substantially as a consequence of decreases in leaf area and roots and increases in runoff. Changes in ET (latent heat flux) revise the surface energy and water budgets, which further affects large-scale atmospheric dynamics and feeds back positively or negatively to long-term forest sustainability. In this study, we used observations from a recent synthesis of 29 pairs of adjacent intact and deforested FLUXNET sites to improve model parameterization of stomatal characteristics, photosynthesis, and soil water dynamics in version 1 of the Energy Exascale Earth System Model (E3SM) Land Model (ELMv1). We found that default ELMv1 predicts an increase in ET after deforestation, likely leading to incorrect estimates of the effects of deforestation on land-atmosphere coupling. The calibrated model accurately represented the FLUXNET observed deforestation effects on ET. Importantly, the search for global optimal parameters converged at values consistent with recent observational syntheses, confirming the reliability of the calibrated physical parameters. Applying this improved model parameterization to the globe scale reduced the bias of annual ET simulation by up to ~600 mm/year. Analysis on the roles of parameters suggested that future model development to improve ET simulation should focus on stomatal resistance and soil water-related parameterizations. Finally, our predicted differences in seasonal ET changes from deforestation are large enough to substantially affect land-atmosphere coupling and should be considered in such studies.

Plain Language Summary Deforestation changes Earth's surface characteristics and affects the water cycle and climate. Although Earth system modeling is an important tool to understand the effects of deforestation, current models have large uncertainties. Here we used FLUXNET-based observations to identify biases in representing deforestation effects on evapotranspiration (ET) in the Energy Exascale Earth System Model (E3SM). Results showed these biases are mostly associated with the representation of trees, not with smaller vegetation types (e.g., grasses). We then used the observations to optimize model parameters and improved simulations of ET and sensible heat fluxes following deforestation. Globally, these improvements led to a reduction in ET bias of 600 mm/year. This improved model allows improved estimates of the effects of deforestation on the water cycle and climate and could benefit forest management and climate adaptation strategies.

1. Introduction

Evapotranspiration (ET) moves water from land to atmosphere and is an important part of the water cycle. ET includes plant transpiration and evaporation from soil, leaf, and water surfaces. By changing water from liquid or solid state to gaseous state, ET consumes a substantial amount of energy (net radiation) absorbed by the land surface. The thermal energy used to drive ET (i.e., latent heat flux, LE) effectively cools the land surface (evaporative cooling, Bonan, 2008; Katul et al., 2012). For this reason, ET is also an important part of the terrestrial energy cycle (Fisher et al., 2011) and land-atmosphere coupling (Koster et al., 2006; Seneviratne et al., 2006; Zeng et al., 2017). The strength of land-atmosphere coupling has been quantified by the evaporative fraction (i.e., the ratio of LE to the sum of LE and sensible heat fluxe, SH), which is affected by transpiration, soil evaporation, and canopy evaporation partitioning (Lawrence et al., 2007).

Different mechanisms drive transpiration and evaporation. Evaporation is determined by surface moisture supply, atmospheric water demand, and surface resistance. Through the opening and closing of their stomata, plants adjust transpiration to regulate temperature, water use, and CO_2 assimilation. Since different plants are associated with different stomata behavior, xylem regulation, and plant hydraulics, transpiration varies dramatically among vegetation types (Dai et al., 2004; Kelliher et al., 1995; Konings & Gentine, 2016).

Human activities have dramatically altered land use and land cover (LULC) over much of the Earth's surface, and these changes are projected to persist. Because of the close relationship between plants and ET, LULC changes are expected to exert large impacts on ET and thus hydrological and biogeochemical cycles and climate (Alkama & Cescatti, 2016; Bonan, 2008; Dirmeyer et al., 2010; Lawrence et al., 2016; Li et al., 2018; Teuling et al., 2010).

Deforestation is one of the most important forms of LULC change (Davin & de Noblet-Ducoudré, 2010; Lawrence & Vandecar, 2015; Lee et al., 2011; Li et al., 2016). The impacts of deforestation on hydrology are relatively well studied at paired catchments at small scale, with a general conclusion that deforestation decreases annual ET and increases land water yields (Brown et al., 2005; Cheng et al., 2017; Yurtseven et al., 2018; Zhang et al., 2001). At large scale, Earth system modeling is an important tool to study the climate effects of deforestation. In the Amazon, for example, a previous study using an Earth System Model (ESM) suggested that a loss of about 40% forest cover of the entire basin might trigger a tipping point (Davidson et al., 2012; Sampaio et al., 2007). Large-scale deforestation beyond this tipping point heavily decreased energy and water released to the atmosphere, which reduced convection and precipitation. In turn, this could lead to a new, drier stable state that makes it difficult to reestablish forests. However, this estimated tipping point is highly uncertain due to the deficiencies in the structure of ESMs (Davidson et al., 2012).

The large uncertainty in ESMs is a long-standing challenge due to the lack of reliable measurements to constrain models. To examine the climate effects of large-scale deforestation, however, deforestation effects on land surface fluxes (particularly ET) need to be correctly parameterized. A new data set of paired FLUXNET (Baldocchi et al., 2001) sites compiled by Chen et al. (2018) allows direct evaluation of the representation of deforestation effects on ET in ESMs. That study paired forest towers with nearby open canopy (e.g., grass and crop) towers and showed that differences in surface fluxes were mostly due to the LULC differences (i.e., deforestation in this case) and that deforestation led to a decrease in annual ET, with large seasonal variability. They also showed that the Community Land Model (CLM, the land component of the Community Earth System Model [CESM]; Oleson et al., 2013) had large ET biases, as has been shown in other studies (Oleson et al., 2004; Swenson & Lawrence, 2014; Tang & Riley, 2013; Wang et al., 2015). These biases led to a poor representation of deforestation effects on ET (Chen et al., 2018). This problem also exists in other ESMs (Pitman et al., 2009).

Since the Energy Exascale Earth System Model (E3SM) was developed based on CESM, we show below that the default E3SM land model (ELMv1) has similarly poor predicted ET responses to deforestation. Therefore, we combined these paired FLUXNET site data with atmospheric forcing data to improve ELMv1 and evaluate biophysical effects of deforestation. Our objectives of this study are to (1) evaluate the representation of deforestation effects on ET in ELMv1; (2) provide a simple solution to improve this misrepresentation by calibrating model parameters; and (3) evaluate implications of this model misrepresentation at site and global scales and recommend next steps for model development.

2. Methodology

2.1. Model Description

E3SM is a new Earth system model supported by the U.S. Department of Energy. It branched from CESM in 2014, with specific version tag 1_3_beta10. The land component ELMv1 branched from the Community Land Model version 4.5 (CLM4.5; Oleson et al., 2013) with specific version tag 4_5_71. Version 1 of E3SM (E3SMv1; Golaz et al., 2019) was released to the public on 23 April 2018. Development in E3SMv1 focused on the water cycles (river flow and water management), biogeochemical cycles, and cryosphere-ocean system (Golaz et al., 2019). In this study, we use the satellite phenology mode of ELMv1, which uses very

similar parameterizations to the biophysical processes in CLM4.5; thus, the performance of ELMv1 analyzed here may also be relevant to CLM.

Here we only describe the equation for calculating stomatal resistance, as we include in-depth analysis of parameter uncertainly associated with the minimum stomatal conductance. Stomatal resistance is calculated using the Ball-Berry conductance model:

$$\frac{1}{r_s} = g_s = m\frac{A_n}{c_s}h_s P_{\text{atm}} + b \tag{1}$$

where r_s is leaf stomatal resistance ($s \cdot m^2 \cdot \mu mol^{-1}$), m is a fitted parameter ($s \cdot m^2 \cdot \mu mol^{-1}$), A_n is leaf net photosynthesis ($\mu mol\ CO_2 \cdot m^{-2} \cdot s^{-1}$), c_s is the CO_2 partial pressure at the leaf surface (Pa), P_{atm} is the atmospheric pressure (Pa), h_s is relative humidity at leaf surface (dimensionless), and b is the minimum stomatal conductance ($\mu mol \cdot m^{-2} \cdot s^{-1}$).

2.2. FLUXNET Data

We used observations from the paired FLUXNET sites compiled by Chen et al. (2018). In each pair, one flux tower is located in a forest (broadleaf or needleleaf; deciduous, evergreen, or mixed; tropical, temperate, or boreal) and the other is in an adjacent land cover type with open canopy (C_3/C_4 grassland, cropland, or open shrub). Due to its important regulation of the global climate, many studies have focused on rapid tropical forest deforestation. However, there were no sites located in the tropics in the original list of paired sites in Chen et al. (2018). Therefore, we added one more pair in the tropics: Sardinilla-Pasture (PA-SPs, an open site) and Sardinilla-Plantation (PA-SPn, a forest site) in Panama (Wolf et al., 2011). In total, our study includes 44 flux towers that make up 29 pairs (Table 1).

Over the list of studied sites, the median straight-line distance between the two sites within each pair is 19.9 km; the median difference in elevation is 20.0 m. Because of their close proximities, the two towers within each pair share very similar atmospheric conditions. However, they are not identical and each tower has their own meteorological measurements (Chen & Dirmeyer, 2016). Chen et al. (2018) demonstrated that the differences in meteorology within each pair, which are generally small, are not the main contributor to the simulated surface flux differences for most of the pairs. Therefore, the differences (open canopy tower minus forest tower) in the observed surface fluxes can be considered largely the effects of deforestation.

Observed eddy covariance meteorological forcing data were used to drive the offline ELMv1. The forcing fields include surface air temperature, precipitation, wind speed, relative humidity, surface pressure, incoming solar radiation, and incoming longwave radiation. All forcing fields were gap-filled by the FLUXNET team using the marginal distribution sampling method. Because this study focuses on surface fluxes, particularly ET (LE) and SH, we used the FLUXNET observed ET for calibration and SH for model evaluation. For evaluation of global simulation of ET, we used the global gridded ET data at $0.5° \times 0.5°$ resolution that was upscaled from site level FLUXNET data (Jung et al., 2009).

2.3. Model Simulations

We conducted two types of model simulations to calibrate and assess the performance of ELMv1 in simulating the biophysical effects of deforestation. The designs of these simulations are described below.

2.3.1. Single-Point Simulations

We ran ELMv1 in the offline mode driven with satellite phenology, which (1) deactivated the prognostic biogeochemical module and (2) prescribed vegetation phenology (i.e., leaf and stem area indices) using the leaf area index data stream created by the CESM model development team and was derived from Moderate-Resolution Imaging Spectroradiometer satellite instrument at 0.5° resolution for each of 15 plant functional types (PFTs, see Table 2 for the PFT numbers, definitions, and their acronyms). The data cover the period from 2001 to 2013, which overlaps with the majority of the data availability of the FLUXNET2015 database. Using this time varying Moderate-Resolution Imaging Spectroradiometer-derived LAI leads to more realistic seasonal and interannual variabilities in ET than from using a static monthly leaf area index (LAI) data set.

We used site level observed atmospheric forcing data to drive the model. The domain (latitude and longitude information of the model grids) and surface data set (vegetation, soil, and other land compositions and their associated properties) were first extracted from the global surface data set (in the predefined model input

Table 1
The Paired Flux Towers Used in This Study

Land cover transition	Pair ID	Site name	Latitude (°N)	Longitude (°E)	Elevation (m)	PFT	Distance (km)	Period
Evergreen needleleaf boreal forests → open shrublands	1	CA-NS2	55.9058	−98.5247	260	2	27.43	2001–2005
		CA-NS6	55.9167	−98.9644	244	11		
	2	CA-NS1	55.8792	−98.4839	260	2	30.25	2001–2005
		CA-NS6	55.9167	−98.9644	244	11		
	3	CA-NS5	55.8631	−98.485	260	2	30.48	2001–2005
		CA-NS6	55.9167	−98.9644	244	11		
	4	CA-NS3	55.9117	−98.3822	260	2	36.29	2001–2005
		CA-NS6	55.9167	−98.9644	244	11		
	5	CA-SF2	54.2539	−105.8775	520	2	19.87	2001–2005
		CA-SF3	54.0916	−106.0053	540	11		
	6	CA-SF1	54.485	−105.8176	536	2	45.41	2003–2006
		CA-SF3	54.0916	−106.0053	540	11		
Evergreen needleleaf boreal forests → croplands	7	DE-Tha	50.9636	13.5669	380	2	8.46	2004–2014
		DE-Kli	50.8929	13.5225	480	15		
	8	DE-Obe	50.7836	13.7196	735	2	18.42	2008–2014
		DE-Kli	50.8929	13.5225	480	15		
Evergreen needleleaf boreal forests → grasslands	9	DE-Tha	50.9636	13.5669	380	2	4.12	2004–2010
		DE-Gri	50.9495	13.5125	385	13		
	10	DE-Obe	50.7836	13.7196	735	2	23.49	2008–2010
		DE-Gri	50.9495	13.5125	385	13		
	11	IT-Ren	46.5869	11.4337	1730	2	59.57	2002–2012
		AT-Neu	47.1167	11.3175	970	13		
Mixed forests → croplands[a]	12	BE-Vie	50.305	5.998	491	2/8	92.82	2004–2014
		BE-Lon	50.5515	4.7461	165	15		
	13	BE-Vie	50.3051	5.9981	493	2/8	69.96	2011–2014
		DE-RuS	50.8659	6.4472	102.76	15		
Evergreen needleleaf temperate forests → open shrublands	14	US-Wi4	46.7393	−91.1663	352	1	16.22	2002–2003
		US-Wi6	46.6249	−91.2982	371	10		
	15	US-Wi0	46.6188	−91.0814	349	1	16.57	2002
		US-Wi6	46.6249	−91.2982	371	10		
	16	US-NC2	35.803	−76.6685	5	1	4.03	2005–2009
		US-NC1	35.8118	−76.7119	5	10		
Deciduous broadleaf temperate forests → open shrublands	17	US-Wi3	46.6347	−91.0987	411	7	15.27	2002–2003
		US-Wi6	46.6249	−91.2982	371	10		
Evergreen needleleaf temperate forests → grasslands	18	NL-Loo	52.1666	5.7436	25	1	46.55	2004–2011
		NL-Hor	52.2404	5.0713	2.2	13		
	19	CZ-BK1	49.5021	18.5369	875	1	0.96	2004–2006
		CZ-BK2	49.4944	18.5429	855	13		
	20	US-Blo	38.8953	−120.6328	1315	1	60.29	2000–2007
		US-Var	38.4133	−120.9507	129	13		
	21	US-Dk3	35.9782	−79.0942	163	1	0.78	2004–2008
		US-Dk1	35.9712	−79.0934	168	13		
	22	US-Fmf	35.1426	−111.7273	546	1	33.91	2006–2010
		US-Fwf	35.4454	−111.7718	2270	13		
Deciduous broadleaf temperate forests → croplands	23	FR-Fon	48.4764	2.7801	90	7	73.3	2005–2013
		FR-Gri	48.8442	1.9519	125	15		
	24	IT-Ro2	42.3903	11.9209	160	7	8.75	2011–2012
		IT-CA2	42.3772	12.026	200	15		
	25	IT-CA1	42.3804	12.0266	200	7	0.36	2011–2013
		IT-CA2	42.3772	12.026	200	15		
	26	IT-CA3	42.38	12.0222	197	7	0.44	2011–2013
		IT-CA2	42.3772	12.026	200	15		
Deciduous broadleaf temperate forests → grasslands	27	US-Dk2	35.9736	−79.1004	168	7	0.68	2003–2008
		US-Dk1	35.9712	−79.0934	168	13		
Evergreen broadleaf temperate forests → grasslands	28	AU-Whr	−36.6732	145.0294	165	5	48.82	2011–2013
		AU-Rig	−36.6499	145.5759	152	13		
Deciduous broadleaf tropical forests → C_4 grasslands	29	PA-SPn	9.3181	−79.6346	78	6	0.59	2007–2009
		PA-SPs	9.3138	−79.6314	68	14		

Note. Six towers are from AmeriFlux: US-Dk1, US-Dk2, US-Dk3, US-Fmf, US-Fwf, US-NC1, US-NC2; all other towers are from the FLUXNET2015 data set. PFT = plant functional type.
[a]We did not plot out this transition group in Figure 3. Instead, we applied 50% each to the transition groups from needleleaf evergreen boreal forests to croplands and from broadleaf deciduous boreal trees to croplands, respectively.

Table 2
Plant Functional Type (PFT) Numbers, Definitions, and Their Acronyms

Code	Plant functional type	Acronym
1	Needleleaf evergreen temperate tree	NET Tmp
2	Needleleaf evergreen boreal tree	NET Brl
3	Needleleaf deciduous boreal tree	NDT Brl
4	Broadleaf evergreen tropical tree	BET Trp
5	Broadleaf evergreen temperate tree	BET Tmp
6	Broadleaf deciduous tropical tree	BDT Trp
7	Broadleaf deciduous temperate tree	BDT Tmp
8	Broadleaf deciduous boreal tree	BDT Brl
9	Broadleaf evergreen shrub	BES
10	Broadleaf deciduous temperate shrub	BDS Tmp
11	Broadleaf deciduous boreal shrub	BDS Brl
12	C_3 arctic grass	C3G Arc
13	C_3 grass	C_3 Grass
14	C_4 grass	C_4 Grass
15	C_3 crop	C_3 Crop

data) based on tower location. Then the PFT compositions were set based on site-specific characterization (Table 1).

For each simulation, ELMv1 was run for 72 years by cycling through the time series of available atmospheric forcings, which varied from 1 to 11 years. We analyzed the model outputs from the last cycle of the available period for analysis, which leaves more than 55 years for the model to reach equilibrium, which is sufficient for hydrological equilibrium in global land models (Cai, Yang, Xia, et al., 2014).

2.3.2. Global Simulations

To demonstrate the impact of model calibration using site level observations on the simulated global ET, we conducted the following experiments: (1) global simulation using default model parameters with present (2010) land use data; (2) global simulation using default model parameters with historical (1960) land use data; (3) global simulation using calibrated model parameters with present land use data; and (4) global simulation using calibrated model parameters with historical land use data. As two examples, we showed the LULC changes between 1960 and 2010 for 8 major PFTs (e.g., tropical broadleaf deciduous tree and C_3 crop) in Figure S1 in the supporting information.

Because five of ELM PFTs were not present in the paired-tower observational synthesis, we extracted additional site data from the FLUXNET2015 data set for those PFTs (Table S1). These sites were used in the calibration for the eight parameters in a similar method (OPT) as for the sites in the paired-tower data set. With these additional PFT calibrations, parameters for all PFTs used in the global ELM simulations were optimized against FLUXNET observations.

All global simulations used the atmospheric forcing data from the Global Soil Wetness Project Phase 3 (Kim, 2017). Each experiment includes 50 simulation years, and the average of last 10 years (2001–2010) was used for analysis.

2.4. Model Calibration

Before model calibration, we first identified influential parameters for ET simulation based on previous studies (Cuntz et al., 2016; Gohler et al., 2013; Jefferson et al., 2017; Ricciuto et al., 2018; Tang et al., 2015). We down selected from this list by changing one parameter at a time and keeping all other parameters at their default values to evaluate impacts on ET simulations (one-at-a-time approach). After these steps, we calibrated the following parameters (Table 3): m (Ball-Berry slope parameter), b (Ball-Berry intercept parameter or minimum stomatal conductance), f_{nr} (fraction of leaf nitrogen in RuBisco), $r_{C:N}$ (leaf carbon/nitrogen [C:N] ratio), θ_{sat} (saturated volumetric soil moisture), K_{sat} (saturated hydraulic conductivity), and Ψ_o and Ψ_c (soil water potential when stomata are fully open or fully closed, respectively). Parameters m and b control

Table 3
Description of Parameters Calibrated in This Study

Parameter	Description	Units	Min	Max	Source
m	Ball-Berry slope parameter	-	4.5	13.5	1
b	Ball-Berry intercept parameter	mmol H2O·m^{-2}·s^{-1}	0	275	1
f_{nr}	Fraction of leaf nitrogen in RuBisco	gN in Rubisco gN^{-1}	0.0231	0.264	1
$r_{C:N}$	Leaf carbon/nitrogen (C:N) ratio	gC/gN	12.5	70	1
θ_{sat}	Saturated volumetric soil moisture	-	0.363	0.489	2
Ψ_o	Soil water potential at full stomatal opening	mm	−83,000	−35,000	3
Ψ_c	Soil water potential at full stomatal closure	mm	−428,000	−224,000	3
K_{sat}	Saturated hydraulic conductivity	mm/s	9.22E−4	0.031	4

Note. The *source* column defines the ranges of the parameters for calibration: (1) physically constrained (parameter values cannot exceed the bounds defined by the *Min* and *Max* columns); (2) ±25% of default values; (3) ±50% of default values; and (4) 1/50 to 50 times of the default values. Since the default parameter values vary by PFT or by site, they are not included here but can be found in Oleson et al. (2013). PFT = plant functional type.

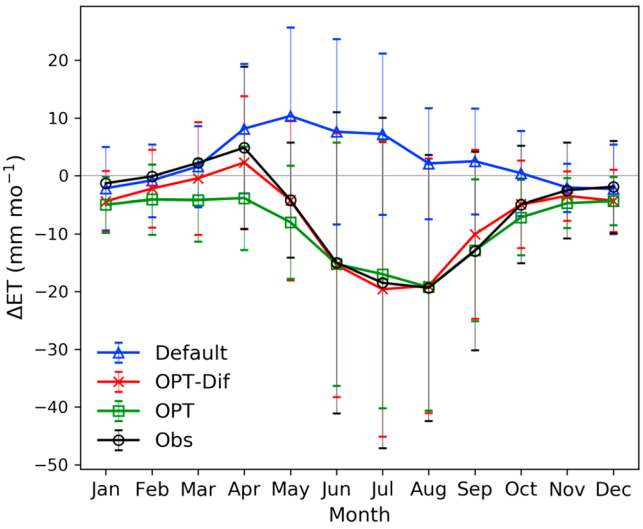

Figure 1. Observed and simulated seasonal cycles of the evapotranspiration (ET) differences between open canopy and forest towers (open-forest), averaged across 29 pairs, showing the effects of deforestation on ET. Error bars indicate the standard deviation among the pairs.

stomatal resistance; f_{nr} and $r_{C:N}$ control photosynthesis; θ_{sat} and K_{sat} control soil moisture content; and Ψ_o and Ψ_c control plant water stress.

To assess the global sensitivity of ELMv1 simulations to these parameters, we used the Sobol sequence sampling technic (Saltelli et al., 2010; Sobol, 2001) to generate parameter samples. The Sobol sequence technic identifies evenly distributed samples from a multidimensional parameter space. The total number of parameter samples (N) is

$$N = n(sD + 2) \tag{2}$$

where n is the number of samples to generate for each specific parameter, s is either 2 if second-order sampling is enabled or 1 otherwise, and D is the number of parameters to be calibrated (eight in this case). Here we used $n = 200$, yielding $N = 2{,}000$ without second-order sampling, which means we ran the model in a single column mode 2,000 times for each tower.

We use the Nash-Sutcliffe efficiency (NSE) coefficient (Nash & Sutcliffe, 1970) to evaluate the goodness of fit between simulations and observations:

$$\mathrm{NSE} = 1 - \sum_{i=1}^{N} (M_i - O_i)^2 / \sum_{i=1}^{N} \left(O_i - \overline{O}\right)^2 \tag{3}$$

where M_i and O_i are the predicted and measured monthly values of the same variable, respectively, and $\overline{O}$ is the mean of the measured values. NSE is minus infinity for a poor fit and 1 for a perfect fit.

We first calibrated parameters for each PFT by averaging the NSE values across different towers associated with the same PFT; this calibration strategy is labeled here as OPT. Given measurement bias, which may be similar for paired towers, and our goal of improving the model-simulated deforestation effects on ET, we added a second calibration strategy (labeled as OPT-Dif) by optimizing the parameters to match the observed difference between the open canopy tower and the forest tower for each pair. The OPT-Dif calibration strategy leverages the idea that differences in paired site measurements may reduce systematic instrument biases present at individual sites. However, OPT-Dif is not a commonly used calibration strategy but is still useful for exploration.

3. Results

Below we first describe results for the paired FLUXNET sites from both observations and simulations and then present results of global simulations.

3.1. Deforestation Effects on ET in Paired FLUXNET Sites

Before model calibration, the default model was unable to capture the deforestation effect at the paired FLUXNET sites, confirming our hypothesis that ELMv1 is biased in handling LULC change, which was also found in previous analyses with CLM4.5 (Figure 1 shows the integrated biases across all sites, Figure 2 shows biases grouped by PFT, and Figure 3 shows biases grouped by type of transition). Observations showed that deforestation resulted in 73.7 mm/year decrease in annual ET, while the default model predicted a 32.9 mm/year increase. The largest observed monthly ET differences between forested and nonforested sites (−19.4 mm/mo) occurred in August, while the default model showed the highest ET difference (+10.4 mm/mo) in May. Therefore, the default model failed to capture the magnitude, timing, and sign of the observed deforestation effects on ET.

The default model relatively accurately simulated the actual ET for open canopy PFTs (on average, annual ET were 411 and 421 mm/year in the default simulation and observations, respectively; Figures 2a–2f). Monthly biases between simulated and observed ET in the open canopy systems were very small for the broadleaf deciduous boreal shrub and C_3 grass. Moderate biases were predicted by the default model for the broadleaf deciduous temperate shrub from February through May, for the C_4 grass, and for the C_3 crop.

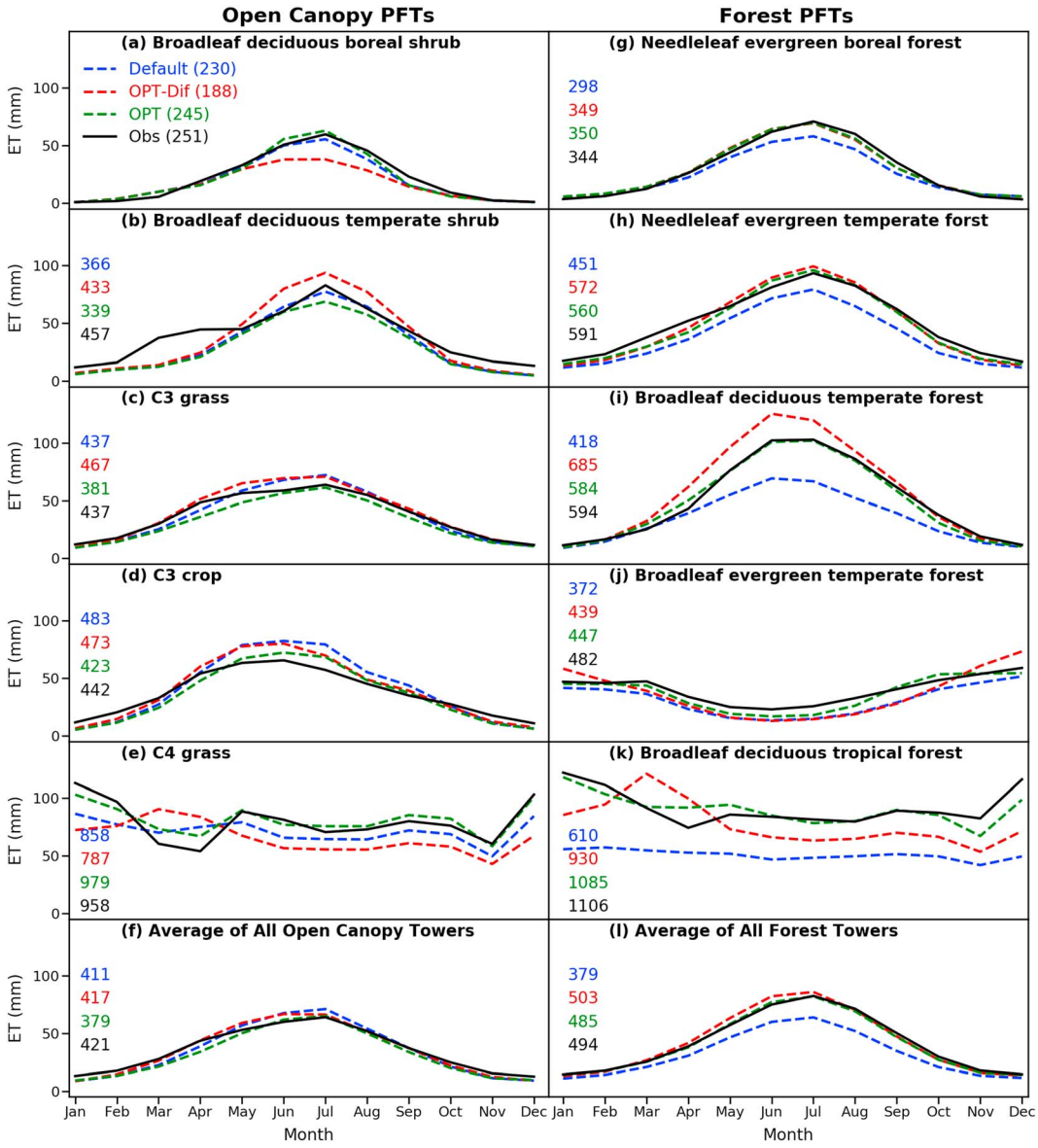

Figure 2. Seasonal cycle of evapotranspiration (mm/mo) by PFTs observed by FLUXNET (black) and simulated by ELMv1 using default parameters (blue), calibrated parameters based on the pair difference (red; OPT-Dif), and calibrated parameters based on individual PFTs (OPT). The left column panels are for open vegetation PFTs, and the right column panels are for forest PFTs. Figures 2f and 2l are the average of the open canopy and forest sites, respectively. The annual mean values are shown on the left on each panel. PTFs = PTF = plant functional types.

Larger biases were found in the forest PFTs (Figures 2g–2l and S2). Simulated annual ET by the default model was lower than observed for all forest PFTs. The largest underestimation is for the broadleaf deciduous tropical tree (610 mm/year vs 1106 mm/year), followed by the broadleaf deciduous temperate tree (418 mm/year vs 594 mm/year), the needleleaf evergreen temperate tree (451 mm/year vs 591 mm/year), and the broadleaf evergreen temperate tree (372 mm/year vs 482 mm/year). The needleleaf evergreen boreal tree had relatively small underestimation (298 mm/year vs 344 mm/year). Overall, the higher the observed annual ET for a particular PFT, the larger the default model bias is. The average of simulated ET across all forest PFTs (Figure S2l) is lower than the average for all open canopy PFTs (Figure S2f), which leads to the overall model bias in the sign of the effect of deforestation on ET (Figure 1).

After calibration with both approaches, model performance was greatly improved for the forest PFTs; while improvements for open canopy PFTs were relatively small (Figure 2). This difference in the benefit of

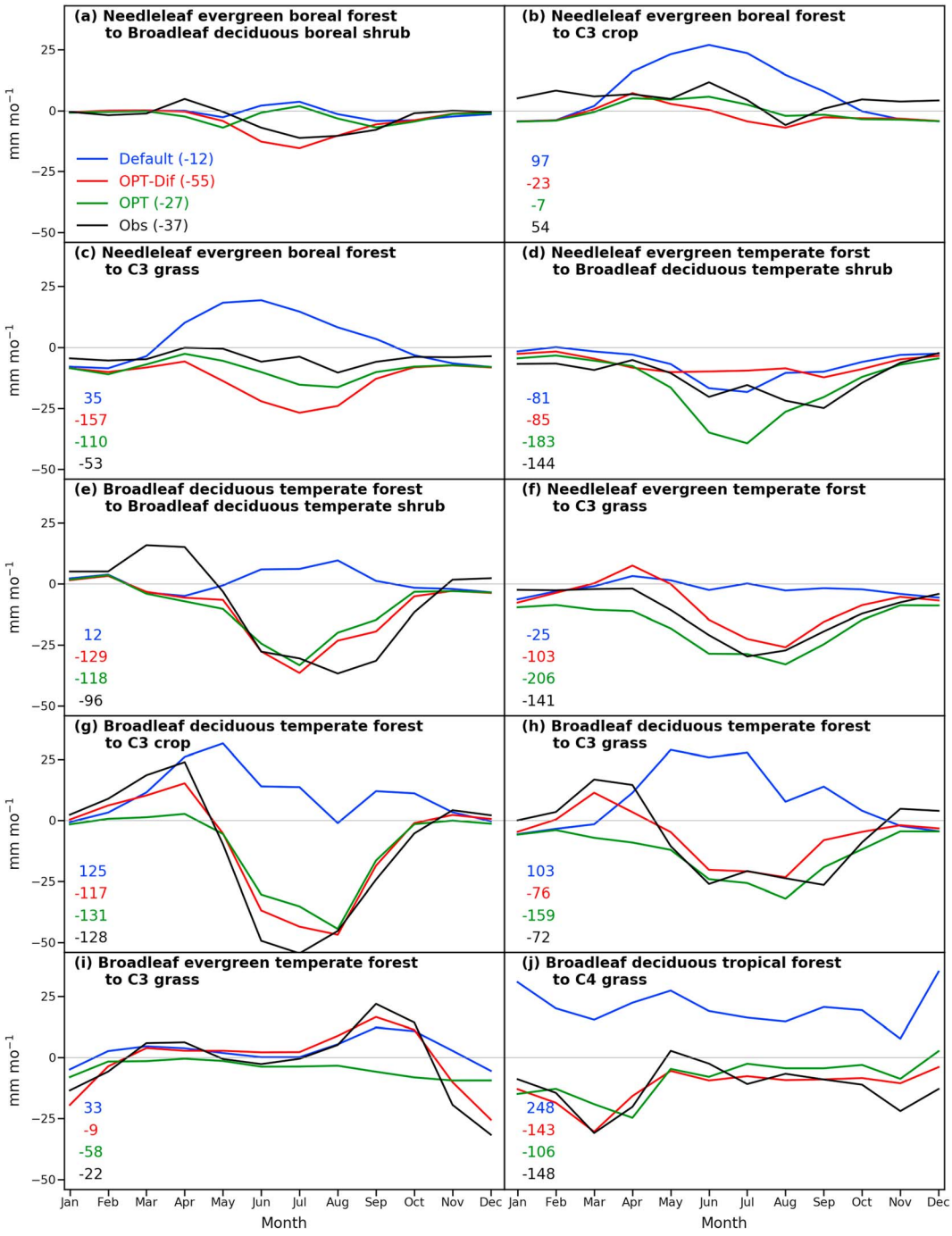

Figure 3. Same as Figure 1 but for each scenario of PFT transitions (changing from one forest PFT to one open canopy PFT). PTF = PTF = plant functional type.

calibration occurred because some PFTs (in particular forest types) are very sensitive to changes in the parameters we selected (e.g., deciduous broadleaf temperate forests) while some PFTs are insensitive (e.g., C_3 grass, see the discussion in section 4.1).

With these improvements, the calibrated model simulations much better represented deforestation effects on ET (Figure 1). The improvements are especially pronounced for summer months (particularly July and August) when deforestation produces the largest reduction in ET. For winter months, discrepancies still

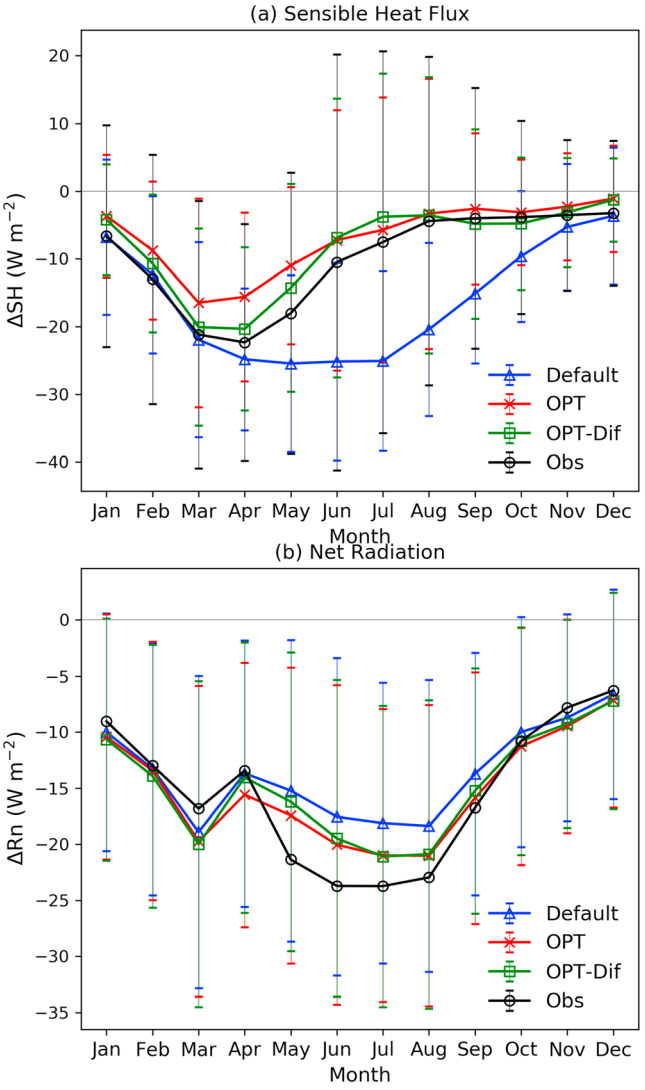

Figure 4. Same as Figure 1 but for sensible heat flux (SH) and net radiation (R_n).

exist in the OPT calibration approach, which is probably due to unidentified secondary influential parameters related to soil evaporation that were not included in the calibration. Interestingly, the default model produced acceptable results against observations for the winter months when the open canopy vegetation and forests have small ET differences. The calibration significantly increased ET reduction in summer months and remained smaller ET reduction in winter months.

Between the two calibration strategies, the OPT-Dif strategy (i.e., calibrating the model using the differences in ET between forested and open canopy sites) led to better model-estimated ET between February and April. Both calibration methods led to comparable improvements in the estimated ET differences from May through October. The observations indicate that deforestation decreased ET primarily and most strongly during the growing season. Deforestation increased ET for about 2 to 3 months before the growing season.

We also evaluated paired site ET differences by grouping similar PFT transitions. ET differences are similar in seasonality with the 29-pair average for 9 out of the 10 groups (i.e., decrease in ET during the growing season, (Figure 3). From observations, only one LULC transition group led to an increase in annual ET (evergreen needleleaf boreal tree to C_3 crop, Figure 3b). Four LULC transition groups showed decreases in annual ET larger than 100 mm/year: needleleaf evergreen temperate tree to open shrub, needleleaf evergreen temperate tree to C_3 grass, broadleaf deciduous tropical tree to C_4 grass, and broadleaf deciduous temperate tree to C_3 crop. In addition to the transition from broadleaf evergreen temperate tree to C_3 grass, all three LULC transition groups that included needleleaf evergreen boreal tree showed smaller decreases or increases due to the low transpiration rate of needleleaf evergreen boreal tree. The two LULC transition groups associated with broadleaf deciduous temperate tree showed moderate ET decreases.

The default model predicted the correct signs of deforestation effects on ET for 4 out of 10 transition groups (Figures 3a, 3b, 3d, and 3f), although the predicted magnitudes of difference poorly match observations. Both model calibration strategies led to the correct sign in ET differences and much better agreement in magnitude and phase for all transition groups, except for the needleleaf evergreen boreal forest to cropland transition (Figure 3b). For that group, although the calibrated model incorrectly predicts the sign, its predictions are closer to observations than the default model for the growing season months.

Between the two calibration strategies, OPT-Dif is better than the OPT method for eight out of the 10 transition groups based on their NSE values that evaluate the fitness of both their means and seasonality, particularly for LULC transition groups a, h, i, and j (Figure 3). But for the LULC transition groups b and c, calibration based on pair differences gives a poorer fit than with the individual PFT calibration method.

3.2. Deforestation Effects on SH and R_n in Paired FLUXNET Sites

We next evaluated changes in the simulated SH due to ET calibration. We found that predicted SH responses to deforestation were also improved (Figure 4a). Both the default and the calibrated models predicted a decrease in SH after deforestation, as suggested by observations. However, the magnitude of decrease was strongly overestimated in the default model, particularly during the summer months. The calibrated models much better captured the magnitude of the observed differences. Between the two calibration methods, OPT-Dif performed better than OPT between March and May.

Similar to ET, calibration mainly improved the SH simulations for the forest PFTs (Figure S3). The default model overestimated SH by 18.7 W/m^2 (59%) for the average of all forest PFTs. The largest overestimation

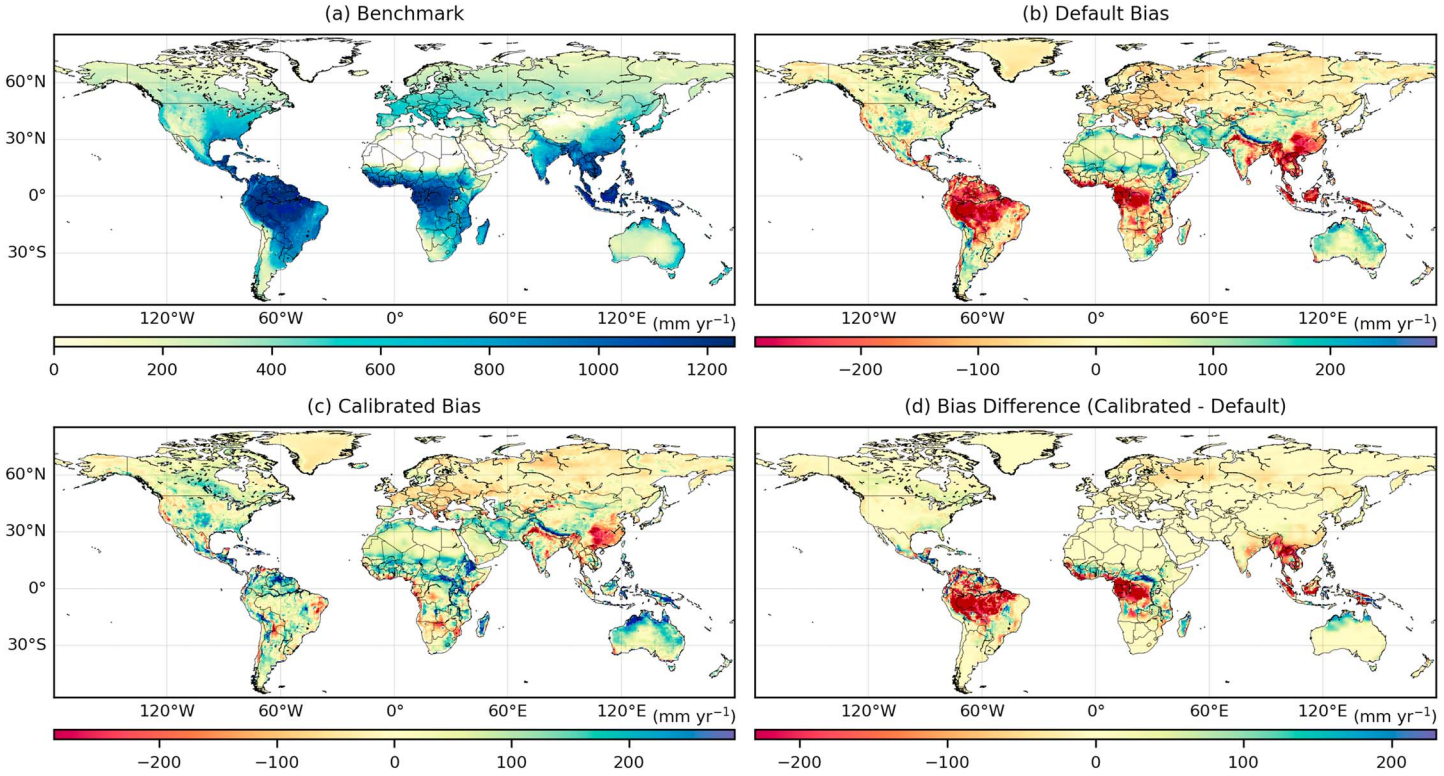

Figure 5. Comparison of global simulations of annual evapotranspiration (mm/year) with observation. (a) Benchmark, (b) bias of the default model, (c) bias of the calibrated model, and (d) difference of absolute bias between calibrated and default model simulations (red: lower bias; blue: higher bias).

was for the tropical broadleaf deciduous tree by 29.7 W/m^2 and for the temperate needleleaf evergreen tree by 28.7 W/m^2. Model calibration made large improvements for these two PFTs and for the temperate broadleaf deciduous tree. Calibration did not substantially affect the open canopy PFT simulations.

In addition, as suggested by the paired tower observations, deforestation reduced the total energy absorbed by land surface (i.e., net radiation, Figure 4b), which is associated with the increase in albedo when changing forests to open canopy vegetation. All model experiments predicted the same sign of change in net radiation as the observations. Overall, modeled changes predicted by the two experiments with calibrated parameters are more consistent with the observation than the default experiment.

3.3. Global Implications

The improved ELMv1 surface ET representations led to large changes in simulated annual global ET, with large latitudinal variation (averaged for 2001–2010; Figure 5). ET biases were reduced with the OPT calibrated parameters, with the largest reduction in the tropical forest regions (Figure 5d). In these regions, the bias reductions might reach 600 mm/year annually. To show a more complete comparison between the default and calibrated (OPT) global simulations, we used the International Land Model Benchmarking system (Collier et al., 2018), which also showed improvement in ET and runoff (Figure S5).

We also analyzed the effects of LULC changes between 1960 and 2010 on ET and the impacts of improvements from model calibration (Figure 6). The default model suggested large annual ET increase for the tropical rain forest regions over this period, with the highest grid cell increase by about 83 mm/year. In contrast, the calibrated model suggested large ET decrease for those regions, with the highest grid cell decrease by about 78 mm/year. These differences led to up to 117 mm/year change in simulated runoff due to LULC changes (Figure S4).

Since the calibrated model is very consistent with the paired FLUXNET observations, the difference between the calibrated and default model simulations can be considered to be an improvement in representing

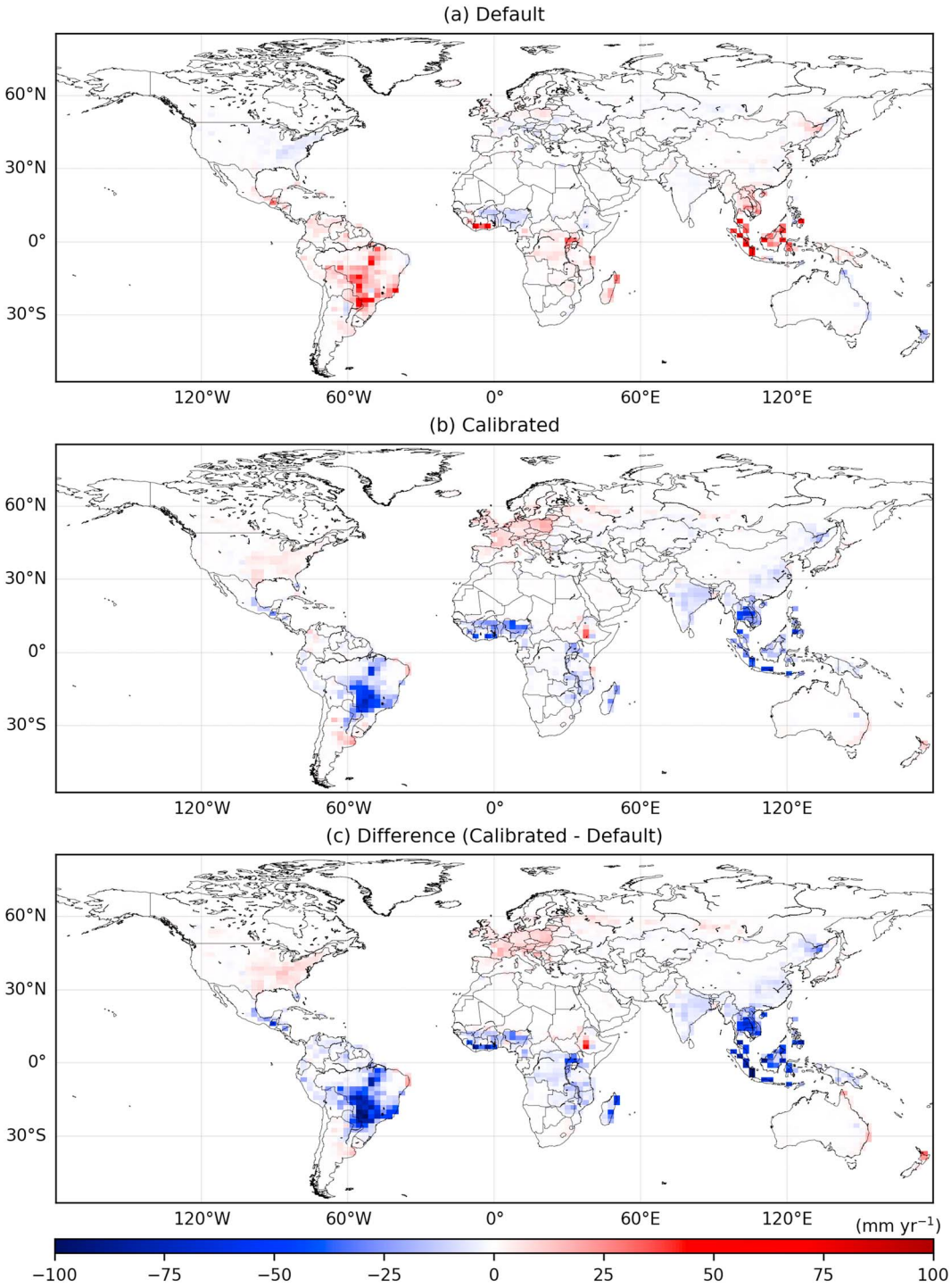

Figure 6. The changes in annual evapotranspiration due to land use and land cover change between 1960 and 2010, as simulated by using the default parameters (a), the calibrated parameters (b), and their difference (calibrate-default) (c). Both simulations are performed with 2001–2010 atmospheric forcings to isolate the effects of the model calibration.

deforestation effects on the surface energy budget. As expected, areas with large differences in predictions are located in tropical rainforests, where LULC changes have been most severe.

Slight increases in ET were simulated for some regions, particularly in Western Europe and Eastern Unites States. This ET increase is due to transitions from croplands to forests that occurred during this period

Table 4
A Comparison of the Ball-Berry Minimum Stomatal Conductance b Among the Default Values Used in ELMv1, Synthesized Values by Lombardozzi et al. (2017, DL2017), and the Optimal Values

Parameter	PFT 1	PFT 2	PFT 5	PFT 6	PFT 7	PFT 10	PFT 11	PFT 13	PFT 14	PFT 15
Default	10	10	10	10	10	10	10	10	40	10
DL2017	17 (21)	8 (-)	34 (28)	129 (41)	73 (84)	130 (146)	–	158 (67)	94 (126)	61 (61)
Calibrated	42	7	45	193	42	19	5	16	188	16

Note. For the synthesized values, the standard deviations are included in the parentheses. PTF = plant functional type.

(Figure S1). These transitions have been reported to change local ET and hence affect the overall energy and water exchanges (Bright et al., 2017; Findell et al., 2017; Teuling et al., 2010). Afforestation in these regions was observed to reduce surface temperature due to the enhanced evaporative cooling effects (Li et al., 2015; Wickham et al., 2012).

4. Discussion

Chen et al. (2018) demonstrated that differences in atmospheric forcings did not substantially affect simulated differences in ET between paired forested and open canopy sites. Therefore, in this section, we discuss other uncertainties and how this study compares to previous studies.

4.1. Parameter Uncertainties

We showed large improvement in representing deforestation effects on ET and SH through calibrating model parameters. We here discuss the meanings of these calibrated parameter values and whether they are physically reasonable. The Ball-Berry intercept (*b*; i.e., minimum stomatal conductance) is a very influential parameter (Findell et al., 2007; van Heerwaarden & Teuling, 2014) and is the only parameter for which observations are available for comparison. In our sensitivity analysis, *b* made the largest contribution to the optimization for 12 out of the 15 PFTs (Table S2). Lombardozzi et al. (2017, hereafter DL2017) compiled observations of *b* for 13 PFTs from 204 data records in previously published studies. We use *b* as an example to analyze uncertainties associated with calibrated parameter values. We note that the Ball-Berry equation was mainly intended to calculate daytime stomatal conductance, while these synthesized values were mostly observed at night. Therefore, we emphasize here the relative values among PFTs.

Our calibrated parameter values are very close to those synthesized by DL2017 for needleleaf evergreen boreal tree (PFT 2), broadleaf evergreen temperate tree (PFT 5), broadleaf deciduous temperate tree (PFT 7), C_4 grass (PFT 14), and C_3 crop (PFT 15), well within the observed standard deviations (Table 4). The optimal values are outside the synthesis uncertainty bounds for needleleaf evergreen temperate tree (PFT 1) and broadleaf deciduous tropical tree (PFT 6). However, their optimal values are not too far from the synthesis uncertainty bounds. Among all PFTs, the calibrated *b* value is the highest for broadleaf deciduous tropical tree (PFT 6); while the synthesized value is the second highest. In addition, there were only two data records for this vegetation type (PFT 6), which is far fewer than for the other vegetation types, implying larger observational uncertainty due to small sample size. Considering the difference in the definition between the model and the synthesis for this parameter, these calibrated values can be considered reasonable for these PFTs.

For broadleaf deciduous temperate shrubs (PFT 10), even though it is within the synthesis uncertainty bound, the optimal *b* value is about 1 order of magnitude smaller than the mean synthesis value. The difference for C_3 grass (PFT 13) is even higher. We found that the discrepancies for these two PFTs are due to the divergent relationships between parameter values and the NSE coefficients among different flux towers categorized as the same PFT. For example, two flux towers are dominated by broadleaf deciduous temperate shrubs: US-NC1 and US-Wi6. In the US-Wi6 tower, across the parameter ensembles, NSE increases with higher *b* values, whereas the opposite pattern occurs in the US-NC1 site (Figure 7). With this contrasting behavior, it is challenging to find parameter values that work well for both flux towers. For this reason, the calibrated model may not appear better than the default model for these two PFTs (Figure 2a), even though the cost function (which weights both towers equally) suggested they were optimal values. We note that the default simulation compared reasonably well with the FLUXNET measurements for this vegetation

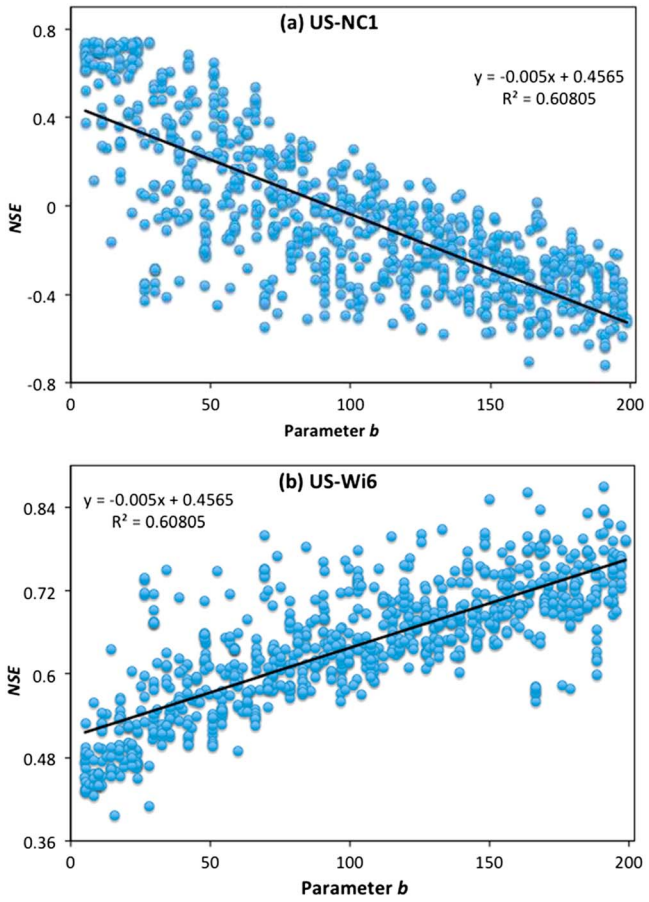

Figure 7. The relationship between Ball-Berry intercept parameter b and the coefficient NSE for (a) the US-NC1 tower and (b) the US-Wi6 tower. Both towers are broadleaf deciduous temperate shrub (PFT 10). PFT = plant functional type.

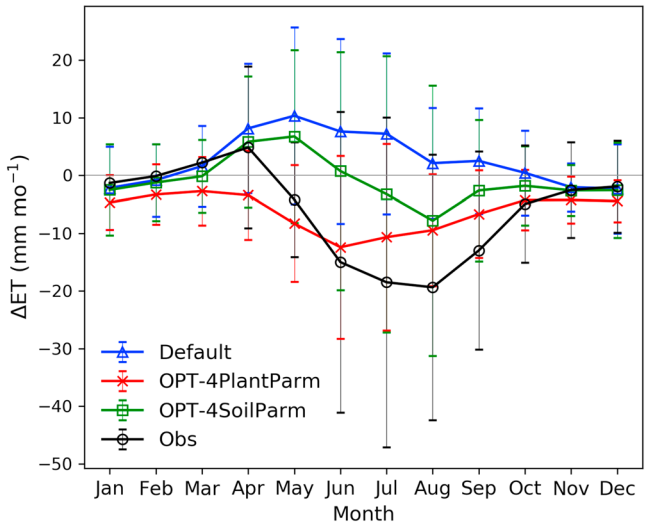

Figure 8. Same as Figure 1 but for the other experiments that only calibrated the four plant parameters (m, b, f_{nr}, and $r_{C:N}$) and the four soil water parameters (θ_{sat}, K_{sat}, Ψ_o, and Ψ_c), respectively.

type. We found the same problem (i.e., disparate effects of b on *NSE* for same-PFT towers) for the C_3 grass towers. For other PFTs, the relationships between b values and NSE are consistent among towers within each PFT.

Bearing in mind parameter uncertainties, we regard these optimal values as reasonable. However, we recognize that the influential parameters used here are not exhaustive. Some other parameters (e.g., rooting depth) may also be influential but have not been identified in either this or previous studies. In addition, 55 FLUXNET sites (44 paired and 11 additional) may not be enough to constraint a global model. Additional sites or other observations may be useful to better constraint such models. Furthermore, calibration may not be the only way to improve the representation of deforestation effects on ET.

4.2. The Role of Soil Property and Soil Water Stress Parameters

We evaluated the stomatal resistance and photosynthesis-related parameters (m, b, f_{nr}, and $r_{C:N}$) known to be important to simulated ET. Calibrating the model using the paired site differences using only these 4 parameters (OPT-4PlantParm) improved the magnitude of simulated ET reduction across all 29 sites compared to the default model (Figure 8). However, the simulated seasonal cycle of ET differences remained biased. Observations suggest the highest ET reduction from deforestation during July and August, while the OPT-4PlantParm calibrated model predicts a maximum in June. Furthermore, the OPT-4PlantParm ET reduction has lower intrayear variability than the observations.

ET depends on plant and soil properties and water availability. Some previous studies found that soil-related parameters are very influential for ET simulations (Cai, Yang, David, et al., 2014; Cuntz et al., 2016). In ELMv1, soil properties are aggregated to global grid cell resolution. Due to the high heterogeneity of soil, it is possible that these properties (i.e., Ψ_o, Ψ_c, θ_{sat}, and K_{sat}) are not representative of the tower locations. By including the soil water-related parameters, the model better captured water availability for ET and thus better represented the ET decrease as a result of deforestation. However, if we only calibrate these four parameters (OPT-4SoilParm), the model was unable to predict a sufficient reduction in ET resulting from deforestation.

4.3. ET Parameterizations in ESMs

ET parameterization plays an important role in climate and ESMs. However, ESMs have large uncertainties in simulating ET, particularly in partitioning ET into its components (e.g., soil evaporation, canopy evaporation, transpiration, and open water body evaporation; Lian et al., 2018; Zeng et al., 2017). Several previous studies proposed to improve soil evaporation estimates in CLM by adding a surface litter layer (Sakaguchi & Zeng, 2009), introducing a new bare-soil evaporation formulation (Tang & Riley, 2013), or replacing the empirical soil resistance parameterization with a dry surface layer (Swenson & Lawrence, 2014). Others proposed to improve vegetation-related processes (Lombardozzi et al., 2017; Tang et al., 2015; Williams et al., 2016). The proposed model changes from these studies all attempted to decrease simulated soil evaporation and increase transpiration. Our calibration also led to higher transpiration to total evapotranspiration ratios (T/ET) for the forested site towers (Figure 9),

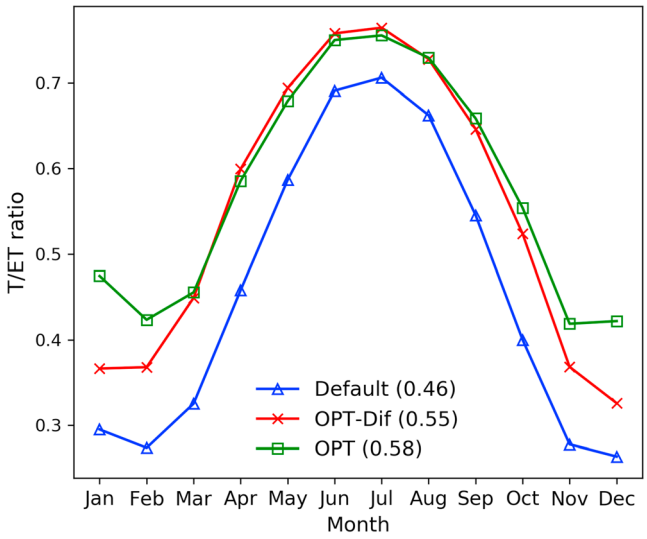

Figure 9. The transpiration to total evapotranspiration ratio (T/ET) before and after calibration for forest towers.

increasing the annual mean ratio from 0.46 to 0.58. This value is closer to the global average of 64 ± 13% estimated by Good et al. (2015). While transpiration is increased, soil evaporation and canopy evaporation stay about the same (Figure S6). For open canopy towers, the changes in T/ET associated with our new calibration are minor. Our calibration results are therefore consistent with efforts to increase the T/ET ratio in ESMs (Lian et al., 2018).

If models are capable of accurately simulating ET for each PFT, they can represent deforestation effects on ET, which is determined by the simulated difference between open canopy land use type and forest land cover type. This study showed that the default ELMv1 misrepresentation of ET differences between forested and open canopy sites was caused primarily by biases in forest land cover type simulations. Therefore, special attention should be paid to systematic biases for different LULC types, particularly for the forest LULC types. For example, even though models can perform satisfactorily for different PFTs, small overestimation for open canopy systems and small underestimation for forest systems may lead to larger errors in their differences compared to observations. This problem makes it challenging to represent the response of deforestation in ESMs. We recommend that models be tested for their responses to perturbations before they are used for relevant scenario analyses, whenever observation allows. As demonstrated in Lawrence et al. (2007) and Williams et al. (2016), improvement for ET simulations involved modifications to a wide range of processes. We show here that model development to improve predicted deforestation effects on ET should focus on characterizing tree stomatal resistance and soil water stress-related processes.

5. Conclusions

Based on previous studies and paired forest and open canopy FLUXNET site data (Chen et al., 2018), deforestation generally decreases ET. We show here that the default ELMv1 has large biases (both in sign and magnitude) in representing these deforestation effects on ET, primarily because of large systematic underestimation of ET for forest land cover types. These biases would likely lead to incorrect inferences of how LULC changes affect surface energy budgets and atmospheric responses. We successfully reduced these biases by calibrating four plant-related and four soil water-related model parameters.

We show that the improved parameterization has significant implications for global surface energy budgets, especially for tropical rainforest regions that have experienced substantial deforestation. Compared to the global observation, the calibrated model reduced the bias of ET simulation by as much as 600 mm/year. Furthermore, the default model-predicted deforestation might cause up to 83 mm/year increase in ET for these regions, while the calibrated model predicted up to a 78 mm/year decrease. The improved model will be useful for better understanding the impacts of human perturbations to the Earth system.

The parameter values from this calibration are reasonable and consistent with previous studies, particularly for minimum stomatal conductance of the Ball-Berry equation. The calibrated parameters increased simulated transpiration for forest land cover types. As a result, the ratio of transpiration to total ET was increased, consistent with recent observation-based assessments and efforts to increase simulated transpiration in ESMs. We recommend stomatal resistance and soil water stress-related processes as foci for future model development to improve ET simulations.

Acknowledgments
This research was supported by the Director, Office of Science, Office of Biological and Environmental Research of the U.S. Department of Energy under contract DE-AC02-05CH11231 as part of their Regional and Global Climate Modeling program through the Reducing Uncertainties in Biogeochemical Interactions through Synthesis and Computation Scientific Focus Area (RUBISCO SFA) project and as part of the Energy Exascale Earth System Model (E3SM) project. FLUXNET atmospheric forcing and surface fluxes data are publically available online (http://fluxnet.fluxdata.org/ and http://ameriflux.lbl.gov/). E3SM model code is open source and available on https://e3sm.org/. E3SM model outputs are available upon request.

References

Alkama, R., & Cescatti, A. (2016). Biophysical climate impacts of recent changes in global forest cover. *Science*, *351*(6273), 600–604. https://doi.org/10.1126/science.aac8083

Baldocchi, D., Falge, E., Gu, L. H., Olson, R., Hollinger, D., Running, S., et al. (2001). FLUXNET: A new tool to study the temporal and spatial variability of ecosystem-scale carbon dioxide, water vapor, and energy flux densities. *Bulletin of the American Meteorological Society*, *82*(11), 2415–2434. https://doi.org/10.1175/1520-0477(2001)082%3C2415:FANTTS%3E2.3.CO;2

Bonan, G. B. (2008). Forests and climate change: Forcings, feedbacks, and the climate benefits of forests. *Science*, *320*(5882), 1444–1449. https://doi.org/10.1126/science.1155121

Bright, R. M., Davin, E., O'Halloran, T., Pongratz, J., Zhao, K. G., & Cescatti, A. (2017). Local temperature response to land cover and management change driven by non-radiative processes. *Nature Climate Change*, *7*(4), 296–302. https://doi.org/10.1038/nclimate3250

Brown, A. E., Zhang, L., McMahon, T. A., Western, A. W., & Vertessy, R. A. (2005). A review of paired catchment studies for determining changes in water yield resulting from alterations in vegetation. *Journal of Hydrology*, *310*(1-4), 28–61. https://doi.org/10.1016/j.jhydrol.2004.12.010

Cai, X., Yang, Z.-L., David, C. H., Niu, G.-Y., & Rodell, M. (2014). Hydrological evaluation of the Noah-MP land surface model for the Mississippi River Basin. *Journal of Geophysical Research: Atmospheres*, *119*, 23–38. https://doi.org/10.1002/2013JD020792

Cai, X., Yang, Z.-L., Xia, Y., Huang, M., Wei, H., Leung, L. R., & Ek, M. B. (2014). Assessment of simulated water balance from Noah, Noah-MP, CLM, and VIC over CONUS using the NLDAS test bed. *Journal of Geophysical Research: Atmospheres*, *119*, 13,751–13,770. https://doi.org/10.1002/2014JD022113

Chen, L., & Dirmeyer, P. A. (2016). Adapting observationally based metrics of biogeophysical feedbacks from land cover/land use change to climate modeling. *Environmental Research Letters*, *11*(3). https://doi.org/10.1088/1748-9326/11/3/034002

Chen, L., Dirmeyer, P. A., Guo, Z. C., & Schultz, N. M. (2018). Pairing FLUXNET sites to validate model representations of land-use/land-cover change. *Hydrology and Earth System Sciences*, *22*(1), 111–125. https://doi.org/10.5194/hess-22-111-2018

Cheng, L., Zhang, L., Chiew, F. H. S., Canadell, J. G., Zhao, F. F., Wang, Y. P., et al. (2017). Quantifying the impacts of vegetation changes on catchment storage-discharge dynamics using paired-catchment data. *Water Resources Research*, *53*, 5963–5979. https://doi.org/10.1002/2017WR020600

Collier, N., Hoffman, F. M., Lawrence, D. M., Keppel-Aleks, G., Koven, C. D., Riley, W. J., et al. (2018). The International Land Model Benchmarking (ILAMB) system: Design, theory, and implementation. *Journal of Advances in Modeling Earth Systems*, *10*, 2731–2754. https://doi.org/10.1029/2018MS001354

Cuntz, M., Mai, J., Samaniego, L., Clark, M., Wulfmeyer, V., Branch, O., et al. (2016). The impact of standard and hard-coded parameters on the hydrologic fluxes in the Noah-MP land surface model. *Journal of Geophysical Research: Atmospheres*, *121*, 10,676–10,700. https://doi.org/10.1002/2016jd025097

Dai, Y., Dickinson, R. E., & Wang, Y.-P. (2004). A two-big-leaf model for canopy temperature, photosynthesis, and stomatal conductance. *Journal of Climate*, *17*(12), 2281–2299. https://doi.org/10.1175/1520-0442(2004)017%3C2281:atmfct%3E2.0.co;2

Davidson, E. A., de Araujo, A. C., Artaxo, P., Balch, J. K., Brown, I. F., Bustamante, M. M. C., et al. (2012). The Amazon basin in transition. *Nature*, *481*(7381), 321–328. https://doi.org/10.1038/nature10717

Davin, E. L., & de Noblet-Ducoudré, N. (2010). Climatic impact of global-scale deforestation: Radiative versus nonradiative processes. *Journal of Climate*, *23*(1), 97–112. https://doi.org/10.1175/2009jcli3102.1

Dirmeyer, P. A., Niyogi, D., de Noblet-Ducoudré, N., Dickinson, R. E., & Snyder, P. K. (2010). Impacts of land use change on climate. *International Journal of Climatology*, *30*(13), 1905–1907. https://doi.org/10.1002/joc.2157

Findell, K. L., Berg, A., Gentine, P., Krasting, J. P., Lintner, B. R., Malyshev, S., et al. (2017). The impact of anthropogenic land use and land cover change on regional climate extremes. *Nature Communications*, *8*(1), 989. https://doi.org/10.1038/s41467-017-01038-w

Findell, K. L., Shevliakova, E., Milly, P. C. D., & Stouffer, R. J. (2007). Modeled impact of anthropogenic land cover change on climate. *Journal of Climate*, *20*(14), 3621–3634. https://doi.org/10.1175/JCLI4185.1

Fisher, J. B., Whittaker, R. J., & Malhi, Y. (2011). ET come home: Potential evapotranspiration in geographical ecology. *Global Ecology and Biogeography*, *20*(1), 1–18. https://doi.org/10.1111/j.1466-8238.2010.00578.x

Gohler, M., Mai, J., & Cuntz, M. (2013). Use of eigendecomposition in a parameter sensitivity analysis of the Community Land Model. *Journal of Geophysical Research: Biogeosciences*, *118*, 904–921. https://doi.org/10.1002/jgrg.20072

Golaz, J.-C., Caldwell, P. M., van Roekel, L. P., Petersen, M. R., Tang, Q., Wolfe, J. D., et al. (2019). The DOE E3SM coupled model version 1: Overview and evaluation at standard resolution. *Journal of Advances in Modeling Earth Systems*, *11*. https://doi.org/10.1029/2018MS001603

Good, S. P., Noone, D., & Bowen, G. (2015). Hydrologic connectivity constrains partitioning of global terrestrial water fluxes. *Science*, *349*(6244), 175–177. https://doi.org/10.1126/science.aaa5931

Jefferson, J. L., Maxwell, R. M., & Constantine, P. G. (2017). Exploring the sensitivity of photosynthesis and stomatal resistance parameters in a land surface model. *Journal of Hydrometeorology*, *18*(3), 897–915. https://doi.org/10.1175/Jhm-D-16-0053.1

Jung, M., Reichstein, M., & Bondeau, A. (2009). Towards global empirical upscaling of FLUXNET eddy covariance observations: Validation of a model tree ensemble approach using a biosphere model. *Biogeosciences*, *6*(10), 2001–2013. https://doi.org/10.5194/bg-6-2001-2009

Katul, G. G., Oren, R., Manzoni, S., Higgins, C., & Parlange, M. B. (2012). Evapotranspiration: A process driving mass transport and energy exchange in the soil-plant-atmosphere-climate system. *Reviews of Geophysics*, *50*, RG3002. https://doi.org/10.1029/2011RG000366

Kelliher, F. M., Leuning, R., Raupach, M. R., & Schulze, E. D. (1995). Maximum conductances for evaporation from global vegetation types. *Agricultural and Forest Meteorology*, *73*(1-2), 1–16. https://doi.org/10.1016/0168-1923(94)02178-M

Kim, H. (2017). Global Soil Wetness Project Phase 3 Atmospheric Boundary Conditions (Experiment 1). Retrieved from: https://doi.org/10.20783/DIAS.501

Konings, A. G., & Gentine, P. (2016). Global variations in ecosystem-scale isohydricity. *Global Change Biology*, *23*(2), 891–905. https://doi.org/10.1111/gcb.13389

Koster, R. D., Guo, Z. C., Dirmeyer, P. A., Bonan, G., Oleson, K. W., Chan, E., et al. (2006). GLACE: The Global Land-Atmosphere Coupling Experiment. Part I: Overview. *Journal of Hydrometeorology*, *7*(4), 590–610. https://doi.org/10.1175/Jhm510.1

Lawrence, D., & Vandecar, K. (2015). Effects of tropical deforestation on climate and agriculture. *Nature Climate Change*, *5*(1), 27–36. https://doi.org/10.1038/nclimate2430

Lawrence, D. M., Hurtt, G. C., Arneth, A., Brovkin, V., Calvin, K. V., Jones, A. D., et al. (2016). The Land Use Model Intercomparison Project (LUMIP) contribution to CMIP6: Rationale and experimental design. *Geoscientific Model Development*, *9*(9), 2973–2998. https://doi.org/10.5194/gmd-9-2973-2016

Lawrence, D. M., Thornton, P. E., Oleson, K. W., & Bonan, G. B. (2007). The partitioning of evapotranspiration into transpiration, soil evaporation, and canopy evaporation in a GCM: Impacts on land-atmosphere interaction. *Journal of Hydrometeorology*, *8*(4), 862–880. https://doi.org/10.1175/Jhm596.1

Lee, X., Goulden, M. L., Hollinger, D. Y., Barr, A., Black, T. A., Bohrer, G., et al. (2011). Observed increase in local cooling effect of deforestation at higher latitudes. *Nature*, *479*(7373), 384–387. https://doi.org/10.1038/nature10588

Li, Y., de Noblet-Ducoudre, N., Davin, E. L., Motesharrei, S., Zeng, N., Li, S. C., & Kalnay, E. (2016). The role of spatial scale and background climate in the latitudinal temperature response to deforestation. *Earth System Dynamics*, *7*(1), 167–181. https://doi.org/10.5194/esd-7-167-2016

Li, Y., Piao, S., Li, L. Z. X., Chen, A., Wang, X., Ciais, P., et al. (2018). Divergent hydrological response to large-scale afforestation and vegetation greening in China. *Science Advances*, *4*(5). https://doi.org/10.1126/sciadv.aar4182

Li, Y., Zhao, M. S., Motesharrei, S., Mu, Q. Z., Kalnay, E., & Li, S. C. (2015). Local cooling and warming effects of forests based on satellite observations. *Nature Communications*, *6*(1), 6603. https://doi.org/10.1038/ncomms7603

Lian, X., Piao, S., Huntingford, C., Li, Y., Zeng, Z., Wang, X., et al. (2018). Partitioning global land evapotranspiration using CMIP5 models constrained by observations. *Nature Climate Change*, *8*(7), 640–646. https://doi.org/10.1038/s41558-018-0207-9

Lombardozzi, D. L., Zeppel, M. J. B., Fisher, R. A., & Tawfik, A. (2017). Representing nighttime and minimum conductance in CLM4.5: Global hydrology and carbon sensitivity analysis using observational constraints. *Geoscientific Model Development*, *10*(1), 321–331. https://doi.org/10.5194/gmd-10-321-2017

Nash, J. E., & Sutcliffe, J. V. (1970). River flow forecasting through conceptual models. Part 1. A discussion of principles. *Journal of Hydrology*, *10*(3), 282–290. https://doi.org/10.1016/0022-1694(70)90255-6

Oleson, K. W., Bonan, G. B., Levis, S., & Vertenstein, M. (2004). Effects of land use change on North American climate: Impact of surface datasets and model biogeophysics. *Climate Dynamics*, *23*(2), 117–132. https://doi.org/10.1007/s00382-004-0426-9

Oleson, K. W., Lawrence, D. M., Bonan, G. B., Drewniak, B., Huang, M., Koven, C. D., et al. (2013). Technical description of version 4.5 of the Community Land Model (CLM) (NCAR Technical Note NCAR/TN-503 + STR). Retrieved from Boulder, Colorado: https://doi.org/10.5065/D6RR1W7M

Pitman, A. J., de Noblet-Ducoudre, N., Cruz, F. T., Davin, E. L., Bonan, G. B., Brovkin, V., et al. (2009). Uncertainties in climate responses to past land cover change: First results from the LUCID intercomparison study. *Geophysical Research Letters*, *36*, L14814. https://doi.org/10.1029/2009GL039076

Ricciuto, D., Sargsyan, K., & Thornton, P. (2018). The impact of parametric uncertainties on biogeochemistry in the E3SM land model. *Journal of Advances in Modeling Earth Systems*, *10*, 297–319. https://doi.org/10.1002/2017MS000962

Sakaguchi, K., & Zeng, X. B. (2009). Effects of soil wetness, plant litter, and under-canopy atmospheric stability on ground evaporation in the Community Land Model (CLM3.5). *Journal of Geophysical Research*, *114*, D01107. https://doi.org/10.1029/2008JD010834

Saltelli, A., Annoni, P., Azzini, I., Campolongo, F., Ratto, M., & Tarantola, S. (2010). Variance based sensitivity analysis of model output. Design and estimator for the total sensitivity index. *Computer Physics Communications*, *181*(2), 259–270. https://doi.org/10.1016/j.cpc.2009.09.018

Sampaio, G., Nobre, C., Costa, M. H., Satyamurty, P., Soares, B. S., & Cardoso, M. (2007). Regional climate change over eastern Amazonia caused by pasture and soybean cropland expansion. *Geophysical Research Letters*, *34*, L17709. https://doi.org/10.1029/2007GL030612

Seneviratne, S. I., Luthi, D., Litschi, M., & Schar, C. (2006). Land-atmosphere coupling and climate change in Europe. *Nature*, *443*(7108), 205–209. https://doi.org/10.1038/nature05095

Sobol, I. M. (2001). Global sensitivity indices for nonlinear mathematical models and their Monte Carlo estimates. *Mathematics and Computers in Simulation*, *55*(1-3), 271–280. https://doi.org/10.1016/S0378-4754(00)00270-6

Swenson, S. C., & Lawrence, D. M. (2014). Assessing a dry surface layer-based soil resistance parameterization for the Community Land Model using GRACE and FLUXNET-MTE data. *Journal of Geophysical Research: Atmospheres*, *119*, 10,299–210,312. http://doi.org/10.1002/2014JD022314

Tang, J., & Riley, W. J. (2013). Impacts of a new bare-soil evaporation formulation on site, regional, and global surface energy and water budgets in CLM4. *Journal of Advances in Modeling Earth Systems*, *5*, 558–571. https://doi.org/10.1002/jame.20034

Tang, J. Y., Riley, W. J., & Niu, J. (2015). Incorporating root hydraulic redistribution in CLM4.5: Effects on predicted site and global evapotranspiration, soil moisture, and water storage. *Journal of Advances in Modeling Earth Systems*, *7*, 1828–1848. https://doi.org/10.1002/2015MS000484

Teuling, A. J., Seneviratne, S. I., Stockli, R., Reichstein, M., Moors, E., Ciais, P., et al. (2010). Contrasting response of European forest and grassland energy exchange to heatwaves. *Nature Geoscience*, *3*(10), 722–727. https://doi.org/10.1038/ngeo950

van Heerwaarden, C. C., & Teuling, A. J. (2014). Disentangling the response of forest and grassland energy exchange to heatwaves under idealized land-atmosphere coupling. *Biogeosciences*, *11*(21), 6159–6171. https://doi.org/10.5194/bg-11-6159-2014

Wang, S. S., Pan, M., Mu, Q. Z., Shi, X. Y., Mao, J. F., Brummer, C., et al. (2015). Comparing evapotranspiration from eddy covariance measurements, water budgets, remote sensing, and land surface models over Canada. *Journal of Hydrometeorology*, *16*(4), 1540–1560. https://doi.org/10.1175/Jhm-D-14-0189.1

Wickham, J. D., Wade, T. G., & Riitters, K. H. (2012). Comparison of cropland and forest surface temperatures across the conterminous United States. *Agricultural and Forest Meteorology*, *166-167*, 137–143. https://doi.org/10.1016/j.agrformet.2012.07.002

Williams, I. N., Lu, Y. Q., Kueppers, L. M., Riley, W. J., Biraud, S. C., Bagley, J. E., & Torn, M. S. (2016). Land-atmosphere coupling and climate prediction over the US Southern Great Plains. *Journal of Geophysical Research: Atmospheres*, *121*, 12,125–12,144. https://doi.org/10.1002/2016JD025223

Wolf, S., Eugster, W., Potvin, C., Turner, B. L., & Buchmann, N. (2011). Carbon sequestration potential of tropical pasture compared with afforestation in Panama. *Global Change Biology*, *17*(9), 2763–2780. https://doi.org/10.1111/j.1365-2486.2011.02460.x

Yurtseven, I., Serengil, Y., Gokbulak, F., Sengonul, K., Ozhan, S., Kilic, U., et al. (2018). Results of a paired catchment analysis of forest thinning in Turkey in relation to forest management options. *Science of the Total Environment*, *618*, 785–792. https://doi.org/10.1016/j.scitotenv.2017.08.190

Zeng, Z. Z., Piao, S. L., Li, L. Z. X., Zhou, L. M., Ciais, P., Wang, T., et al. (2017). Climate mitigation from vegetation biophysical feedbacks during the past three decades. *Nature Climate Change*, *7*(6), 432–436. https://doi.org/10.1038/nclimate3299

Zhang, L., Dawes, W. R., & Walker, G. R. (2001). Response of mean annual evapotranspiration to vegetation changes at catchment scale. *Water Resources Research*, *37*(3), 701–708. https://doi.org/10.1029/2000WR900325